physica status solidi

pss

www.interscience.wiley.com

reprints

www.pss-rapid.com

www.pss-c.com

www.pss-b.com

www.pss-a.com

WILEY-VCH

REPRINT

Phys. Status Solidi A **206**, No. 9, 2177–2181 (2009) / **DOI** 10.1002/pssa.200881789

physica status solidi a
www.pss-a.com
applications and materials science

Semimagnetic semiconductor oxides as materials for transparent electronics and spintronics

A. I. Savchuk*, **V. P. Makhniy, V. I. Fediv, G. I. Kleto, and S. A. Savchuk**

Chernivtsi National University, Kotsyubynsky Street 2, 58012 Chernivtsi, Ukraine

Received 19 September 2008, revised 2 January 2009, accepted 16 March 2009
Published online 28 July 2009

PACS 68.35.Ct, 68.37.Ps, 68.55.ag, 78.20.Ls, 78.66.Hf, 85.75.–d

* Corresponding author: e-mail a.savchuk@chnu.edu.ua, Phone: +38 0372 584 755, Fax: +38 0372 552914

Zinc oxide-based semimagnetic semiconductor (SMS) ZnMnO, ZnMnFeO and ZnMnSnO thin films were deposited on sapphire and glass substrate by pulsed laser deposition (PLD) and RF sputtering techniques. Further, ZnMnO nanocrystals embedded in polyvinyl alcohol (PVA) and polyvinyl pyrrolidone (PVP) matrices were prepared by chemical method employing zinc acetate and manganese acetate as precursors. The morphology of the thin films was studied using atomic force microscopy (AFM). Large variety of the morphology images was obtained depending on the film composition and growth conditions. The most interesting feature was observed for the ZnMnSnO films, in which the formation of clusters including nanowire-like structures was shown. Optical transmission spectra suggest that metals Mn, Fe and Sn substitute for Zn^{2+} ions in the ZnO lattice, resulting in the increase in the band gap energy. Magneto-optical Faraday rotation measurements confirm ferromagnetic ordering in ZnMnFeO thin films and paramagnetic behaviour for the other films.

1 Introduction Doping of transition metals (TM) in ZnO results in the formation of oxide-based semimagnetic semiconductors (SMSs) or diluted magnetic semiconductors (DMSs). These materials have became especially attractive after theoretical prediction of room temperature ferromagnetism in ZnO doped with Mn [1]. Namely for this reason new functionality can be added to conventional oxides and application in spintronic devices can be realized [2–6]. It is very important for spintronic application that magnetism has intrinsic nature and not associate with secondary phase structures. Numerous research groups have reported on experimental evidence of ferromagnetic ordering in oxide SMS [7–14], but its exact origin and mechanisms are still under discussion. Mechanisms of superexchange, double exchange, free-carrier-mediated exchange and exchange through bound magnetic polaron have been involved to explain the ferromagnetic ordering above room temperature [15–21]. It was shown in our previous studies that $Zn_{1-x}Mn_xO$ single crystals and thin films demonstrate paramagnetic behaviour [22, 23], whereas for $Zn_{1-x-y}Mn_xFe_yO$ thin films ferromagnetism was experimentally confirmed [24]. In this work, we report on complex study of electrical, structural, optical and magneto-optical properties of ternary and quaternary SMS oxides in form of thin films and nanocrystals.

2 Experimental Thin films of SMS oxides under investigations were deposited by using two different techniques. For the deposition of ternary $Zn_{1-x}Mn_xO$ ($0 \le x \le 0.1$) thin films pulsed laser deposition (PLD) technique was applied. An ultrahigh vacuum chamber with a base pressure of 10^{-7} Pa was a key element of the used PLD set-up. The XeCl excimer laser ($\lambda = 308$ nm, $\tau = 30$ ns) was operated at a repetition rate of 10 Hz. Optimal laser fluence was measured to be about 5.5 J/cm^2. The film thickness was controlled by the number of laser pulses.

Deposition of quaternary co-doped $Zn_{1-x-y}Mn_xFe_yO$ and $Zn_{1-x-y}Mn_xSn_yO$ thin films have been performed by RF-diode sputtering technique with planar cathode and 1.76 MHz power source in argon–oxygen gas mixture. The ratio of sputtering power, substrate temperature and oxygen content in gas mixture were those critical parameters, which mainly

affected structural and electrical properties of the films deposited by this technique.

Composite targets for both technological methods were prepared by pressing technique with using of ZnO, Mn_3O_4, Fe_3O_4 and SnO_2 pure powders as initial components. Two different kinds of substrates (glass and sapphire) have been used in both the methods. The substrate temperature could be varied from 20 to 300 °C.

$Zn_{1-x}Mn_xO$ nanocrystals embedded in polymer matrix were prepared by chemical method. As a source of Zn^{2+} and Mn^{2+} ions served zinc acetate ($ZnAc_2 \cdot 4H_2O$) and manganese acetate ($MnAc_2 \cdot 4H_2O$), respectively. Then 15 mL of H_2O_2 solution (30%) was added. After reaction for more than 10 h with continuous strong stirring at the boiling point of water, the solution was filtered and dried at 90 °C. As a polymer matrix for oxide nanoparticles was used the mixture of polyvinyl alcohol (PVA) and polyvinyl pyrrolidone (PVP).

The surface morphology of oxide layers was investigated by atomic force microscopy (AFM) system, which can operate in semicontact mode, error mode and phase contrast.

Optical transmission and absorption spectra were measured in range of 0.2–25 μm at temperatures of 4.2–300 K. Magneto-optical Faraday rotation was measured in range of 0.4–0.7 μm in magnetic field up to 50 kOe.

3 Results and discussion

3.1 Electrical and magnetic characteristics In the Table 1, we have summarized main electrical and magnetic characteristics of the grown thin films.

The electrical properties were probed by four-point probe resistance and Hall measurements. Undoped ZnO as a rule exhibits n-type conductivity that can be explained by the inner defects. It is well known, that the oxygen vacancy and the zinc interstitial act as donors, while the zinc vacancy and the oxygen antisite act as acceptors. Therefore, electron type of conduction in undoped ZnO is determined the relation between several kinds of defects. In particular, Zn excess at interstitial sites can provide donor states.

For the quaternary oxide with composition $Zn_{0.88}Mn_{0.05}Fe_{0.07}O$ we have observed p-type of conductivity and room temperature ferromagnetic behaviour.

We suggest, that in this case the introducing of Mn and Fe in ZnO lattice leads to the change of relation between native defects to side of those defects which give acceptor states.

Table 1 Main electrical and magnetic characteristics.

film composition	conductivity type	resistivity (Ω cm)	magnetism
ZnO	n	10^7	dia
$Zn_{1-x}Mn_xO$ (vacuum)	n	10^6	para
$Zn_{1-x}Mn_xO$ (oxygen)	n	10^7	para
$Zn_{1-x-y}Mn_xFe_yO$	p	10^4	ferro
$Zn_{1-x-y}Mn_xSn_yO$	n	10^4	para

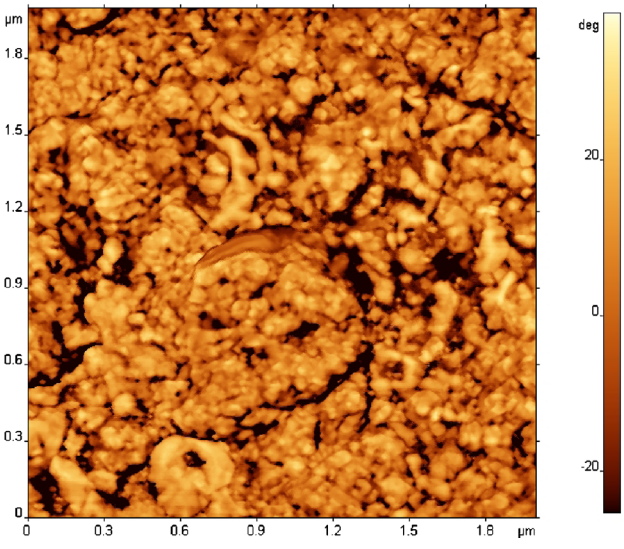

Figure 1 (online color at: www.pss-a.com) AFM micrograph (phase contrast) of $Zn_{0.9}Mn_{0.1}O$ thin film deposited by PLD on sapphire substrate.

Electrical resistivity was also found to decrease in the case of Mn, Sn co-doping. In addition, it was found for the $Zn_{0.9}Mn_{0.1}O$ film that the presence of pure oxygen atmosphere during PLD deposition leads to increase in electrical resistivity, *i.e.* explained by decrease in the oxygen vacancy concentration.

3.2 AFM characterization The surface morphology of the layers studied by AFM shows strong dependence on deposition technique and conditions. The most homogenous surface was found for $Zn_{0.9}Mn_{0.1}O$ thin films grown by PLD on sapphire substrate at temperature of 300 °C (Fig. 1). It should be noticed that for this kind of samples surface roughness is increased, when pure oxygen atmosphere during deposition is created into chamber. The surface of $Zn_{0.9}Mn_{0.1}O$ film sample grown at oxygen ambient has a maximum height of 30.62 nm and a root mean square (Rms) roughness of 4.31 nm.

Surface morphology of quaternary thin films is characterized more complicated AFM images. The most interesting feature was observed for $Zn_{0.93}Mn_{0.03}Sn_{0.04}O$ thin films deposited by RF sputtering on glass substrate at room temperature. From Figs. 2 and 3, we can see that this kind of deposition gives rise to the formation of elongated clusters, which in turn consist of nanowires with average length of a few micrometers and average diameter of a few tenth of nanometers.

The layer height for the $Zn_{0.93}Mn_{0.03}Sn_{0.04}O$ film shown in Fig. 3 is about 3 nm and the Rms roughness is 1.5 nm.

The observed nanowire-like structures have not certain orientation in plane of film surface, but they are oriented only along the surfaces.

3.3 Optical and magneto-optical spectra The observed optical transmission spectra of oxide SMS thin

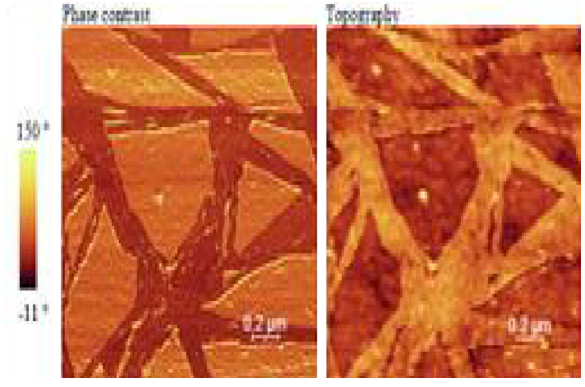

Figure 2 (online color at: www.pss-a.com) AFM micrographs (phase contrast and topography) of $Zn_{0.93}Mn_{0.03}Sn_{0.04}O$ thin film deposited by RF sputtering on glass substrate at 300 °C.

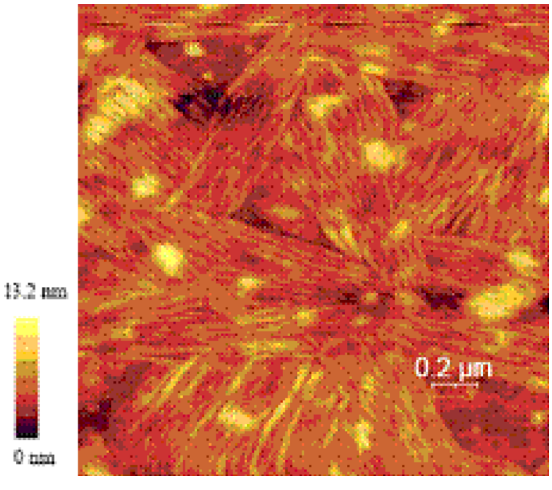

Figure 3 (online color at: www.pss-a.com) AFM image (topography) of $Zn_{0.93}Mn_{0.03}Sn_{0.04}O$ thin films showing presence of nanowire-like nanostructures.

films with different compositions have typical form near band gap absorption edge. The absorption edge is shifted towards the lower wavelength side with the increase in Mn, Fe and Sn content. Obviously, this is indication that the band gap E_g of the materials increases with the doping concentration of the used impurity ions.

As an example, Fig. 4 shows optical transmission spectra of $Zn_{0.9}Mn_{0.1}O$, $Zn_{0.93}Mn_{0.03}Sn_{0.04}O$ and $Zn_{0.88}Mn_{0.05}Fe_{0.07}O$ thin films at liquid helium temperature. From this figure, we can see that the absorption edge is more abrupt and shifted towards the lower wavelength side for $Zn_{0.9}Mn_{0.1}O$ sample. The estimated values of band gap E_g for $Zn_{0.93}Mn_{0.03}Sn_{0.04}O$, $Zn_{0.88}Mn_{0.05}Fe_{0.07}O$ and $Zn_{0.9}Mn_{0.1}O$ films are 3.54, 3.52 and 3.48 eV, respectively. From temperature studies of the $Zn_{0.9}Mn_{0.1}O$ sample, we have estimated the temperature coefficient of band gap $dE_g/dT = 0.4$ meV/K.

In order to evaluate transparency of the oxide SMS thin films, we have performed optical measurements in infrared region up to wavelength 25 μm. Appropriate transmission

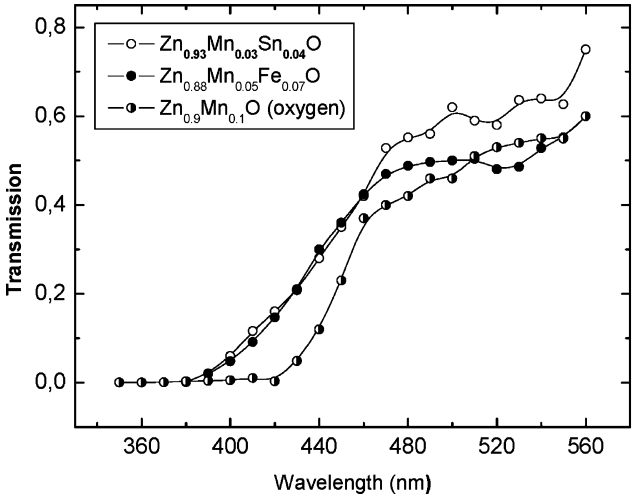

Figure 4 Transmission spectra of the oxide SMS films with different compositions.

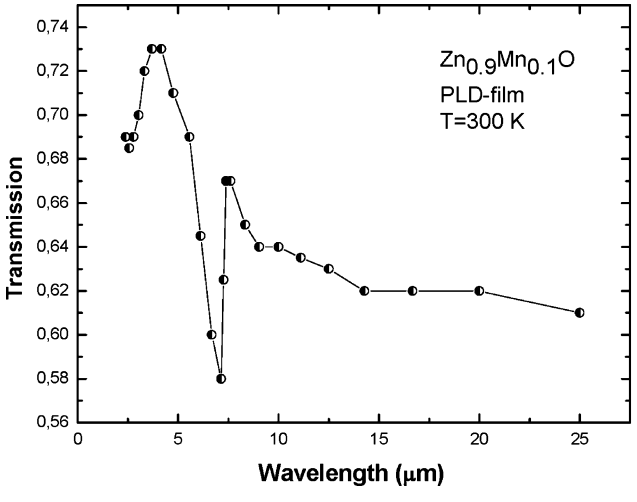

Figure 5 Transmission spectrum of $Zn_{0.9}Mn_{0.1}O$ thin film deposited by PLD on sapphire substrate in infrared region.

spectrum for $Zn_{0.9}Mn_{0.1}O$ thin film is shown in Fig. 5. It was found that the value of transmission coefficient is slowly decreased with increase in wavelength. In addition, it was observed in infrared region the absorption band with maximum at 7.32 μm (0.169 eV). Presently origin of this absorption band is unclear.

Previous studies of magneto-optical Faraday effect in oxide SMS bulk crystals and thin films [22–24] allowed to find paramagnetic behaviour in ternary $Zn_{1-x}Mn_xO$ and ferromagnetic ordering in $Zn_{0.88}Mn_{0.05}Fe_{0.07}O$ thin films. The present results confirm room temperature ferromagnetism in co-doped $Zn_{0.88}Mn_{0.05}Fe_{0.07}O$ thin films, but suggest of absence of similar magnetic behaviour for new quaternary $Zn_{0.93}Mn_{0.03}Sn_{0.04}O$ oxides. The latter is characterized the other conductivity type (n-type) and it is possible reason for the exhibition of paramagnetic state.

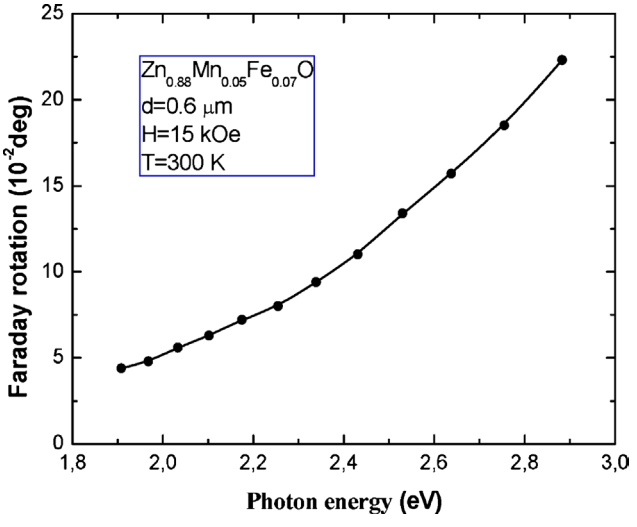

Figure 6 Spectral dependence of the Faraday rotation for $Zn_{0.88}Mn_{0.05}Fe_{0.07}O$ thin film on glass substrate.

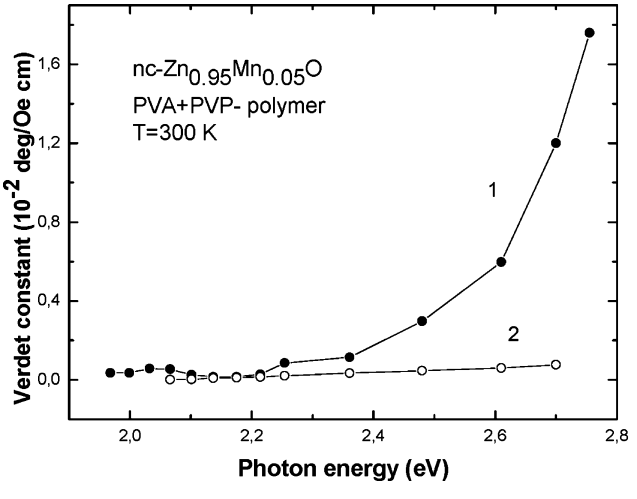

Figure 7 Spectral dependence of the Faraday rotation for $Zn_{0.95}Mn_{0.05}O$ nanocrystals embedded in polymer matrix (curve 1) and polymer film without nanoparticles (2).

Spectral dependence of the Faraday rotation for $Zn_{0.88}Mn_{0.05}Fe_{0.07}O$ thin films, shown in Fig. 6, is in good correlation with appropriate optical absorption spectra.

For $Zn_{0.95}Mn_{0.05}O$ nanocrystal samples, it was observed typical spectral dependence of the Faraday rotation (Fig. 7), but the position of the edge in this spectrum as well as the absorption edge is shifted towards higher photon energy because of confinement effect in SMS nanoparticles.

4 Conclusions Thin films of SMS oxides such as $Zn_{1-x}Mn_xO$, $Zn_{1-x-y}Mn_xFe_yO$ and $Zn_{1-x-y}Mn_xSn_yO$ were fabricated by PLD and RF sputtering techniques. Nanocrystals of $Zn_{1-x}Mn_xO$ oxides were prepared by using simple method of colloidal chemistry. The observed AFM images demonstrate different surface morphology including exhibition of nanowire-like structures. Optical transmission spectra suggest of blue shift of the absorption edge and increase in band gap E_g with increase in content of impurity ions. The estimated values of E_g for $Zn_{0.9}Mn_{0.1}O$, $Zn_{0.88}Mn_{0.05}Fe_{0.07}O$ and $Zn_{0.93}Mn_{0.03}Sn_{0.04}O$ films are 3.48, 3.52 and 3.54 eV, respectively. High transparency is shown for SMS oxides in infrared region. Faraday rotation spectra have typical for SMS materials character and indicate different magnetic behaviour depending on film composition. Further experimental studies are in progress in order to elucidate the connection between the observed nanostructures in AFM images and magnetism of SMS oxides.

Acknowledgements The work has been supported in part by the Ministry of Education and Science of Ukraine.

References

[1] T. Dietl, H. Ohno, F. Matsukura, J. Cibert, and D. Ferrand, Science **287**, 1019 (2000).
[2] S. J. Pearton, C. R. Abernathy, D. P. Norton, A. F. Hebard, Y. D. Park, L. A. Boatner, and J. D. Budai, Mater. Sci. Eng. **R 40**, 137 (2003).
[3] A. W. Prelier, A. Fouchet, and B. Mercey, J. Phys.: Condens. Matter **15**, R1583 (2003).
[4] S. J. Pearton, W. H. Heo, M. Ivill, D. P. Norton, and T. Steiner, Semicond. Sci. Technol. **19**, R59 (2004).
[5] S. A. Chambers, Surf. Sci. Rep. **61**, 345 (2006).
[6] F. Pan, C. Song, X. J. Liu, Y. C. Yang, and F. Zeng, Mater. Sci. Eng. **R 62**, 1 (2008).
[7] P. Sharma, A. Gupta, F. J. Owens, A. Inoue, and K. V. Rao, J. Magn. Magn. Mater. **282**, 115 (2004).
[8] Y. M. Kim, M. Yoon, I.-W. Park, and J. H. Lyou, Solid State Commun. **129**, 175 (2004).
[9] M. Diaconu, H. Schmidt, H. Hochmuth, M. Lorenz, G. Benndorf, J. Lenzner, D. Spemann, A. Setzer, K.-W. Nielsen, P. Esquinazi, and M. Grundmann, Thin Solid Films **486**, 117 (2005).
[10] J. Zhang, R. Skomski, and D. J. Sellmyer, J. Appl. Phys. **97**, 10D303 (2005).
[11] A. C. Mofor, A. El-Shaer, A. Bakin, and A. Waag, Appl. Phys. Lett. **87**, 062501 (2005).
[12] J. Zhang, R. Skomski, and D. J. Sellmyer, J. Appl. Phys. **97**, 10D303 (2005).
[13] D. P. Joseph, G. S. Kumar, and C. Venkateswaran, Mater. Lett. **59**, 2720 (2005).
[14] C. Liu, B. Xiao, F. Yun, H. Lee, U. Ozgur, Y. T. Moon, H. Morkoc, M. Abouzaid, and P. Ruterana, Superlattices Microstruct. **39**, 124 (2006).
[15] M. H. F. Sluiter, Y. Kawazoe, P. Sharma, A. Ionue, A. R. Raju, C. Rout, and U. V. Waghmare, Phys. Rev. Lett. **94**, 187204 (2005).
[16] M. S. Park, S. K. Kwon, and B. I. Min, Phys. Rev. B **65**, 161201 (2002).
[17] K. Sato, and H. Katayama-Yoshida, Phys. Status Solidi B **229**, 673 (2002).
[18] D. A. Schwartz, and D. R. Gamelin, Adv. Mater. **16**, 2115 (2004).

[19] P. V. Radovanovic, and D. R. Gamelin, Phys. Rev. Lett. **91**, 157202 (2003).
[20] J. M. D. Coey, A. P. Donvalis, C. B. Fitzgerald, and M. Venkatesan, Appl. Phys. Lett. **84**, 1332 (2004).
[21] J. Osterwalder, T. Droubay, T. Kaspar, J. Williams, C. M. Wang, and S. A. Chambers, Thin Solid Films **484**, 289 (2005).
[22] A. I. Savchuk, P. N. Gorley, V. V. Khomyak, K. S. Ulyanytsky, S. V. Bilichuk, A. Perrone, and P. I. Nikitin, Mater. Sci. Eng. B **109**, 196 (2004).
[23] A. I. Savchuk, V. I. Fediv, S. A. Savchuk, and A. Perrone, Superlattices Microstruct. **38**, 421 (2005).
[24] A. I. Savchuk, V. I. Fediv, G. I. Kleto, S. V. Krychun, and S. A. Savchuk, Phys. Status Solidi A **204**, 106 (2007).